Power losses Analysis in Frequency Domain of IPMSM Drive fed by Cascaded H-Bridges Multilevel Inverter

Claudio Nevoloso[1], Antonino Oscar Di Tommaso[1], Rosario Miceli[1], Gioacchino Scaglione[1],
[1]Department of Engineering, University of Palermo
Viale Delle Scienze, Building nr.9
90128 Palermo, Italy
E-Mail: claudio.nevoloso@unipa.it

Salvatore De Caro[2], Salvatore Foti[2], Antonio Testa[2]
[2]Department of Engineering, University of Messina
Contrada di Dio
98158 Sant'Agata , Messina, Italy

Acknowledgements

This work was supported in part by the Prin 2017-Settore/Ambito di intervento: PE7 linea C Advanced power-trains and -systems for full electric aircrafts under Grant 2017MS9F49 and in part by the Sustainable Mobility Center (Centro Nazionale per la Mobilità Sostenibile—CNMS) under Grant CN00000023 CUP B73C22000760001.

Keywords

«PMSM drives», «CHBMI», «Power losses», «MC-PWM», «Power measurement».

Abstract

Power losses analysis of an IPMSM drive is a challenging task, especially, when multilevel inverters are employed. This study focuses on an IPMSM drive fed by a Cascaded H-Bridges Multilevel Inverter (CHBMI) controlled by MC-PWM strategies, employing a frequency domain power analysis approach based on Discrete Fourier Transform (DFT).

Introduction

Electric drive systems represent one of the largest end-consumers of electrical energy and a significant increase in energy consumption is expected in the future due to the use of more and more transportation electrification, automotive and industrial drives [1]. In this context, the conventional two-level Voltage Source Inverters (VSIs) are the most employed commercial technologies used in adjustable-speed drive applications. They allow motor soft-starting capabilities, accurate torque, speed and position controls with motor operations even at partial load maintaining reasonable energy-saving benefits [2]. The main drawback is correlated to the pulse-width-modulated voltage waveforms that generate high-frequency harmonics on both voltage and currents, causing significant additional power losses with respect to sinusoidal supply, which reduces motor efficiency, producing noise, vibrations and heat [3]-[4].
In this scenario, industrial and academic researchers pushed their efforts towards the optimization of electric drives performances by reducing the motor power losses both with hardware and software solutions [5]-[8]. Furthermore, the standardization bodies have recently released various standards [9]-[10] concerning power losses measurements of electrical drives and by defining the energy efficiency indicators for Power Drive Systems (PDSs), Complete Drive Modules (CDMs) and motors. Therefore, the motor efficiency requirements are going to become stricter over time, thus resulting in power losses reduction in both the motor and the whole power drive system.
A possible solution for motor drive power losses reduction is related to the use of Multilevel Inverters (MIs), a very widespread application in all fields that require higher voltages with respect to those provided by three-leg inverters (such as in electric railway traction, automotive, industrial drives, etc.). Indeed, the MIs output voltage presents also a natural reduced harmonic content

with respect to the PWM voltage of conventional two-level inverters. This behaviour provides a further reduction of harmonic current components, which results in very low torque ripple, copper and iron losses reduction, smoother rotational speed, few vibrations and noise.
Although power losses analysis, measurement procedures and related prescriptions for adjustable-speed drives fed by conventional two-level VSI are widely discussed in literature [11]-[14], the same aspects are not much deeply debated in the case of MIs-fed PMSM drives. Furthermore, it is necessary to consider that the motor power losses are a function of a multitude of events, among which the most important are: the motor load conditions, its electrical and mechanical parameters, the adopted modulation strategy and the switching frequency.
In this paper, the authors propose to transfer a method of power loss analysis, used in [15]-[16] for three-leg inverter drives and based on frequency domain power analysis, to the case of IPMSM fed by CHBMI. Some experimental tests have been carried out and their results and comments are here provided for the validation of the proposed analysis method. In this analysis, the CHBMI-fed IPMSM drive is controlled with two different Multi-Carrier PWM (MC-PWM) techniques, namely: the Sinusoidal Phase Shifted (SPS) and the Sinusoidal Phase Disposition (SPD), each characterized by a different voltage harmonic content [17]. Moreover, in order to investigate also the impact of switching frequency on motor power losses, experimental tests have been performed by considering three different switching frequency values. In this regard, the frequency domain power analysis approach is used and the IPMSM power losses have been detected for different working conditions and classified in fundamental and harmonic losses.

Power analysis in the frequency domain

Electric active power is determined by means of sampled voltages and currents with the following expression:

$$P = \frac{1}{N}\sum_{k=0}^{N-1} v_k\, i_k \quad (1)$$

where N is the number of acquired samples and v_k and i_k represent the *k-th* sample of the instantaneous voltage and current, respectively. The electrical active power P can also be calculated, with the same results, by applying the Discrete Fourier Transform (DFT). In this case, the total input power is obtained by applying the following formula:

$$P = P_{DC} + \sum_{h=1}^{\frac{N}{2}-1} V_h\, I_h cos(\varphi_h) \quad (2)$$

where P_{DC} is the DC power, V_h and I_h represent the RMS values of the *h-th* order voltage and current harmonic, respectively, and φ_h represents their mutual phase displacement. Equation (2) shows that the active power is generated only by voltage and current harmonic components at the same frequency. This approach considers all harmonic components, including subharmonics and interharmonics. Therefore, the total active input power of a three-phase electrical motor can be calculated by summing the one absorbed by each phase, i.e., by

$$P_{input} = P_{ina} + P_{inb} + P_{inc} \quad (3)$$

The total active power can be defined as the sum of fundamental power, calculated with fundamental voltage and current components, and harmonic power as follow:

$$P_{input} = P_1 + P_{harm} \quad (4)$$

By considering that the high-frequency harmonics have negligible impact on torque production, the fundamental power losses ΔP_1 and the harmonic power losses ΔP_{harm} can be determined by means of the following relationships:

$$\Delta P_1 = P_1 - P_m \quad (5)$$

$$\Delta P_{harm} = P_{input} - P_m - \Delta P_1 = P - P_1 \quad (6)$$

where P_1 is the fundamental active power and P_m is the mechanical power. The total power losses can be calculated as:

$$\Delta P = P_{input} - P_m = \Delta P_1 + \Delta P_{harm} \quad (7)$$

The fundamental and harmonic power losses percentage values have been considered and calculated by the following relationships:

$$\Delta P_1[\%] = \frac{\Delta P_1}{\Delta P} \quad (8)$$

$$\Delta P_{harm}[\%] = \frac{\Delta P_{harm}}{\Delta P} \quad (9)$$

Furthermore, particular care has been paid to the determination of fundamental quantities and related phase displacement, therefore, it is necessary to consider the leakage spectrum phenomenon and set the observation time in order to obtain an appropriate frequency resolution. For this reason, in this work, the observation time and

the related sampling frequency have been set equal to 1 s and 1 MHz, respectively, by obtaining a frequency resolution of 1 Hz and the acquisition of an integer number of current and voltage waveform periods. In this way, spectrum leakage side effects can be neglected.

IPMSM drive and test bench

The CHBMI under test is a three-phase five-level prototype, whose circuit diagram is depicted in Fig. 1.

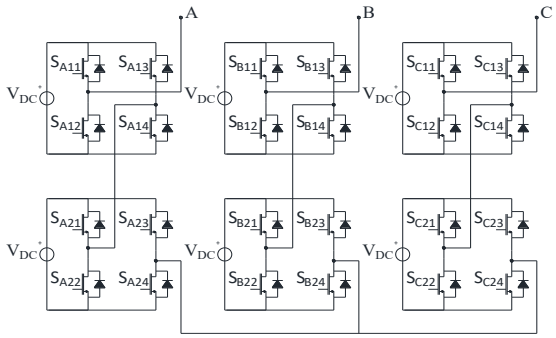

Fig. 1 Three-phase five-level CHBMI circuit diagram.

In order to perform the IPMSM accurate power loss detection, a test rig, shown in Fig. 2, has been designed and set up at the SDESLab of the University of Palermo. It is composed by:

- a three-phase IPMSM with interior SmCo PMs, whose main data are reported in Table I and its parameters described in [17];
- a three-phase five-level CHBMI MOSFET-based inverter obtained by assembling six power H-bridges, whose main technical data are reported in Table II;
- six programmable DC power supplies RSP-2400, with rated voltages of 48 V whose main technical data are reported in [19];
- a Teledyne LeCroy MDA 8038HD oscilloscope equipped with high-voltage differential probes Teledyne Lecroy HVD3106A 1 kV, 120 MHz, and high sensitivity current probes Teledyne Lecroy CP030A AC/DC, 30 A RMS, 50 MHz;
- a Delta Ohm temperature probe model DO 9847 for temperature monitoring purposes.

The IPMSM drive is controlled by a Field Oriented Control (FOC) strategy, whose block diagram is reported in Fig. *3*, implemented on a System on Module (SOM) sbRIO 9651 composed of an ARM Cortex-A9 processor and an Artix7 FPGA unit programmable in the Labview graphic language. This control strategy presents a closed-loop control of speed and currents performed by the use of digital PI controllers. The i_d current has been set equal to 0 A for simplicity and because flux weakening operations are not considered in this work. This choice is the optimal solution for comparison purposes. The load torque is applied by a Magtrol hysteresis brake (Model HD-715-8NA), coupled to the shaft of the motor and controlled by a digital dynamometer controller (Magtrol DSP6001). The peculiar feature of the FOC control consists in the possibility to vary the adopted modulation strategy and its switching frequency f_{sw}. In this regard, the output voltages obtained by the FOC are modulated with two different MC-PWM modulation strategies.

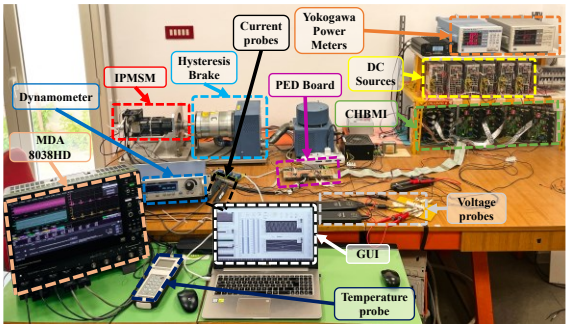

Fig. 2 Test rig.

Table I: IPMSM nameplate data

Quantity	Symbol	Value
Rated Voltage	V_n	132 V
Rated current	I_n	3.6 A
Nominal Speed	n	4000 rpm
Maximum Speed	n_{max}	6000 rpm
Nr. of pole pairs	P	3
Nr. of phases	M	3
Nominal torque	T_{emn}	1.8 Nm
Peak torque	T_{emmax}	9.2 Nm

Table II: CHBMI MOSFET-based-IRFB4115PBF DATA

Quantity	Symbol	Value
Voltage	V_{dss}	150 V
Resistance	R_{DSon}	9.3 mΩ
Current	I_D	104 A
Turn on delay	T_{Don}	18 ns
Rise time	Tr	73 ns
Turn off delay	T_{Doff}	41 ns
Fall time	T_F	39 ns
Reversal recovery	T_{RR}	86 ns

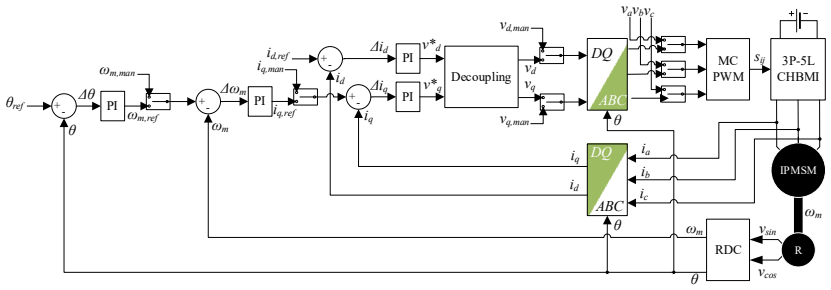

Fig. 3 FOC scheme diagram.

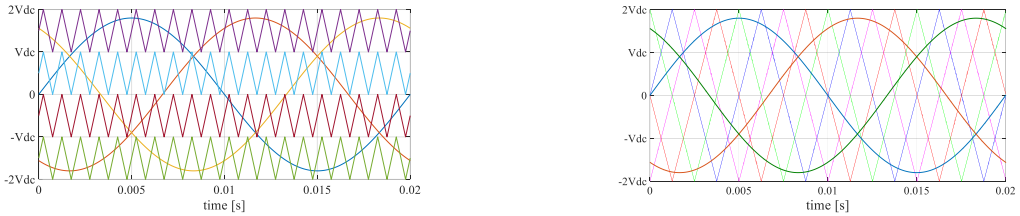

(a) (b)

Fig. 4 MC-PWM strategies employed: (a) SPD, (b) SPS.

The MC-PWM strategies are obtained by considering PD and PS modulation schemes with Sinusoidal (S) modulation signals, whose characteristic signals are shown in Fig. *4*. These modulation strategies have been chosen because they present different behaviour in terms of voltage harmonics spectra and are the most diffused and suitable in electric drives application [20]. In detail, SPD modulation presents voltage harmonics centered at the switching frequency and integer multiplies, whereas SPS modulation presents harmonics centered at four times of the switching frequency and integer multiplies [18].

The accurate detection of input and output IPMSM active powers is performed by Teledyne LeCroy MDA 8038HD oscilloscope. To reduce power angle errors and to obtain a consequently reduced value of the related uncertainties, a deskew calibration source DCS025 has been employed for phase angle calibration of voltage and current signals. The dynamometer controller Magtrol DSP6001 provides torque and speed signals that are acquired by MDA 8038HD oscilloscope. The experimental investigations have been carried out for several IPMSM working points chosen according to standard IEC-61800-9-2 [10]. The standard provides eight different measurement points in the speed-torque plane as a function of rated torque and speed. In this work, an additional point has been considered for a total of nine IPMSM working points. The IPMSM operation at the rated speed of 4000 rpm is obtained with a modulation index value higher than 1. Therefore, to avoid CHBMI overmodulation operation, the IPMSM maximum working speed has been limited to 3000 rpm. The test points are depicted in Fig. *5*. Each experimental test has been performed at IPMSM thermal equilibrium whose constant temperature has been detected with the temperature probe.

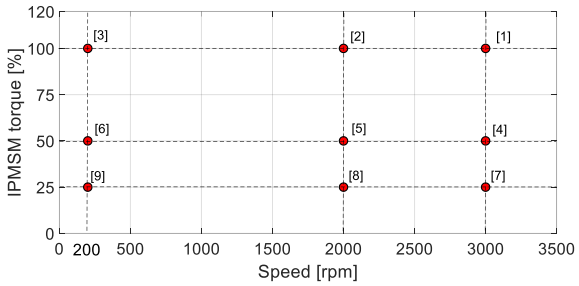

Fig. 5 IPMSM measurement points.

Experimental results

As described previously, the experimental investigations have been carried out by considering nine IPMSM working points, using first SPS and, then the SPD modulation strategies and repeated for switching frequency values equal to 8, 12 and 16 kHz, respectively. Therefore, a huge amount of data have been acquired and analyzed. By way of example, the IPMSM voltage and current quantities acquired at working point 2, where the fundamental frequency is 100 Hz, with f_{sw} equal to 8 kHz are reported in Fig. *6*. By applying the DFT approach, the related cumulative IPMSM input active powers percentage value trends in the frequency domain are reported in Fig. *7*(a)-(b).

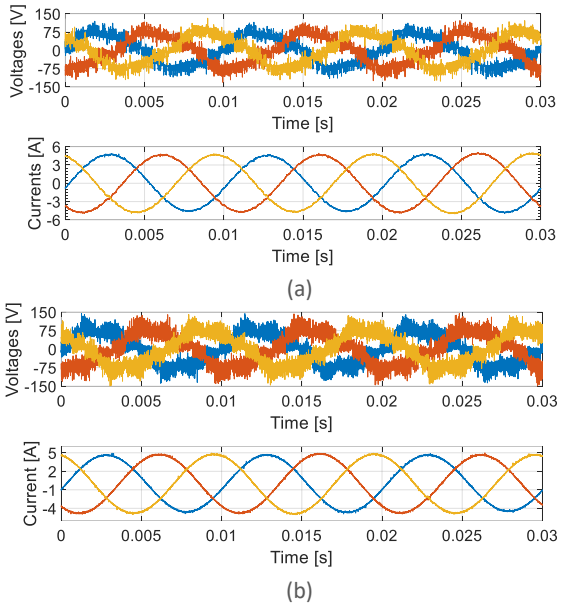

Fig. 6 IPMSM voltage and current quantities at working point 2: (a) SPD, (b)SPS.

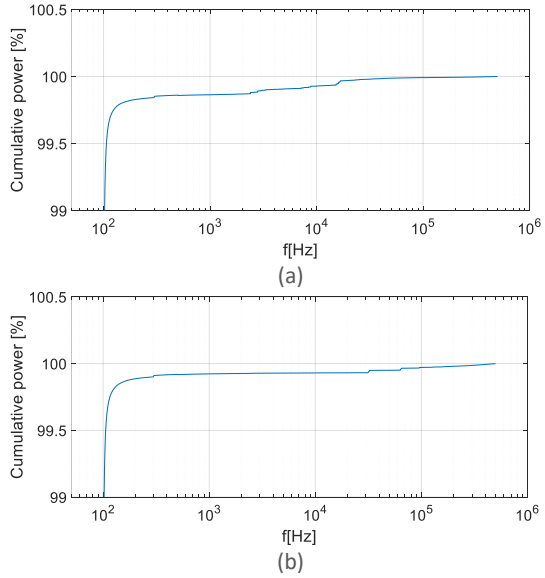

Fig. 7 IPMSM input active power trend in the frequency domain: (a) SPD, (b) SPS.

As expected, due to the use of CHBMI to feed the IPMSM, more than 99% of IPMSM input active power is centered at the fundamental frequency. However, due to the different harmonic content between the modulation strategies considered, it is possible to observe different values of input cumulative power at the fundamental frequency and the related increases occur in different frequency ranges. The IPMSM total power losses detected for the nine IPMSM working conditions, for each switching frequency value considered and for the SPD and SPS modulation are reported in Table III and Table IV, respectively. For repeatability purposes, the measurements of IPMSM power losses have been performed three times and no significant differences have been detected (in the worst case 0.2% respect to the mean value between the three measurements).

Table III: IPMSM total power losses detected with SPD

	ΔP [W]		
SPD	f_{sw}=8 kHz	f_{sw}=12 kHz	f_{sw}=16 kHz
1	126.66	122.97	122.38
2	112.38	112.09	112.25
3	90.03	90.06	90.09
4	57.95	57.1	57.05
5	44.13	44.51	44.27
6	24.63	24.64	24.42
7	37.02	37.06	37.09
8	25.44	25.6	25.41
9	8.11	8.12	8.1

Table IV: IPMSM total power losses detected with SPS

	ΔP [W]		
SPS	f_{sw}=8 kHz	f_{sw}=12 kHz	f_{sw}=16 kHz
1	115.28	114.67	114.38
2	104.52	103.21	103.77
3	84.4	82.91	82.64
4	52.85	52.64	52.46
5	40.91	40.65	40.7
6	23.05	22.81	22.62
7	34.16	34.2	34.29
8	23.44	23.5	23.24
9	7.43	7.41	7.29

It is possible to observe that the IPMSM presents lower power losses when it is controlled with the SPS modulation strategy. This behaviour can be attributed to the SPS voltage harmonic spectrum that is positioned at a higher frequency range value with respect to the SPD and, thus, it results in a more reduced current harmonic content. Regarding the switching frequency influence, in both modulation strategies, an overall IPMSM power losses reduction has been detected from 8 kHz to 12 kHz, whereas no significant power losses reduction has been detected from 12 kHz to 16 kHz. In order to perform an accurate power losses analysis in the frequency domain, the total power losses ΔP value detected for the nine IPMSM working conditions, the relative fundamental power losses ΔP_1 [%] and harmonic power losses ΔP_{harm} [%] for each switching frequency values considered are reported in Fig. 8-10, respectively.

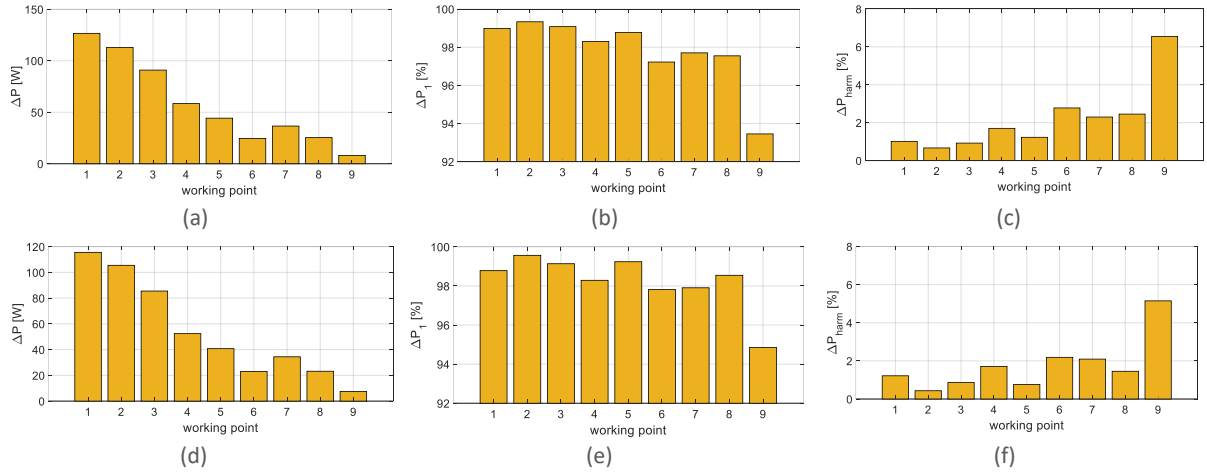

Fig. 8 Power loss analysis at 8 kHz: (a) total power losses SPD, (b) percentage fundamental power losses SPD, (c) percentage harmonic power losses SPD, (d) total power losses SPS, (e) percentage fundamental power losses SPS, (f) percentage harmonic power losses SPS.

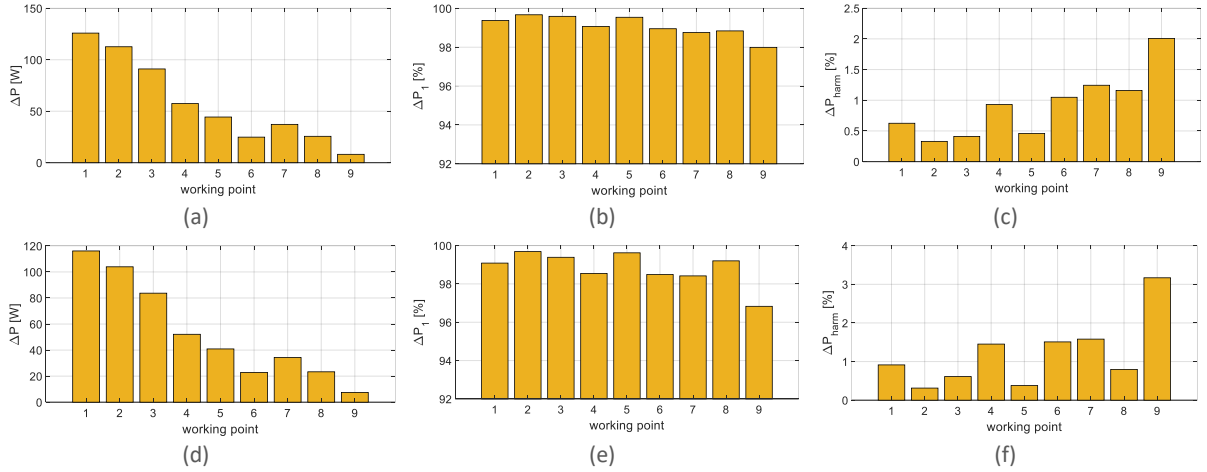

Fig. 9 Power loss analysis at 12 kHz: (a) total power losses SPD, (b) percentage fundamental power losses SPD, (c) percentage harmonic power losses SPD, (d) total power losses SPS, (e) percentage fundamental power losses SPS, (f) percentage harmonic power losses SPS.

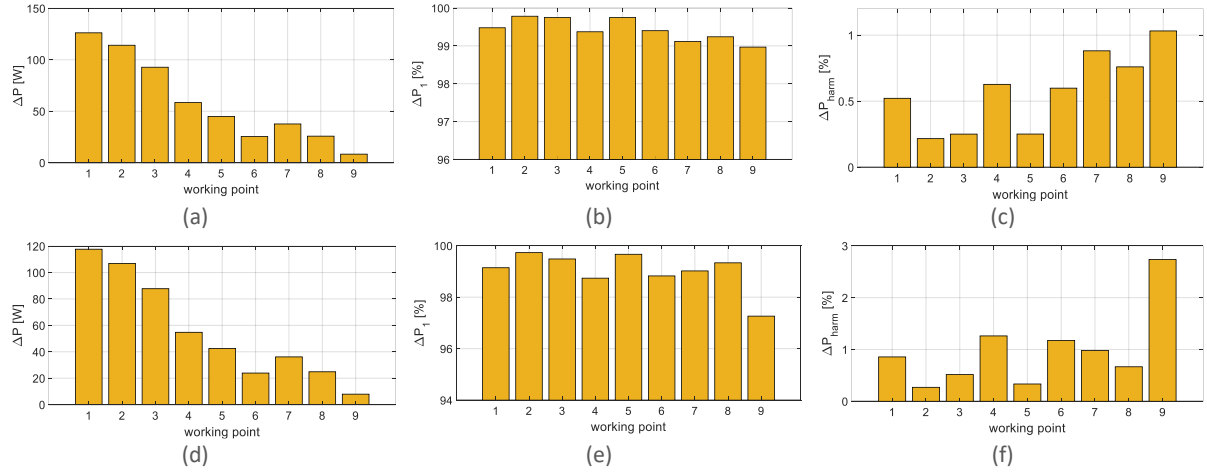

Fig. 10 Power loss analysis at 16 kHz: (a) total power losses SPD, (b) percentage fundamental power losses SPD, (c) percentage harmonic power losses SPD, (d) total power losses SPS, (e) percentage fundamental power losses SPS, (f) percentage harmonic power losses SPS.

In both modulation strategies, it is possible to highlight a reduction of the harmonic power losses in percentage value as the switching frequency increases and a consequence increase of fundamental power losses in percentage values. In particular, at f_{sw} equal to 16 kHz, the harmonic power losses are less than or equal to 1% in all IPMSM working conditions when SPD modulation strategy is used. The experimental analysis carried out on the IPMSM drive fed by CHBMI shows that the vast majority of IPMSM power losses are generated by the fundamental electrical quantities. Furthermore, the increase in switching frequency value generates an overall reduction of harmonic power losses percentage values, but it is necessary to consider that the increase in switching frequency values increases CHBMI power losses. Since the typical IPMSM loss minimization control algorithms reduce the fundamental power losses and the CHBMI are high-efficiency systems, the study conducted allows to state significant margins for an overall performance improvement of IPMSM drives fed by CHBMI in terms of efficiency compared to the conventional IPMSM drives fed with two-level VSIs.

Conclusion

This paper presents an experimental power losses analysis in the frequency domain of an IPMSM fed by CHBMI controlled with SPD and SPS modulation strategies. Experimental investigations have been carried out for nine IPMSM working conditions, in steady state thermal equilibrium and for three different switching frequency values. The analysis performed shows that the IPMSM presents lower power losses when the SPS modulation strategy is employed and this result can be related to the high-frequency bandwidth of voltage harmonics generated. Furthermore, a power losses analysis distribution in terms of fundamental power losses and harmonic power losses, expressed in percentage values, has been carried out by varying the switching frequency. The results obtained show a progressive reduction of harmonic power losses as the switching frequency increase in both modulation strategies. Therefore, by taking into account that the main source of reduction in electric drive efficiency is linked to motor losses, an overall increase in the efficiency of the IPMSM drive fed by CHBMI can be obtained by the reduction of fundamental losses that generally are the power losses controllable.

References

[1]. F. J. T. E. Ferreira and A. T. de Almeida, "Reducing Energy Costs in Electric-Motor-Driven Systems: Savings Through Output Power Reduction and Energy Regeneration," in *IEEE Industry Applications Magazine*, vol. 24, no. 1, pp. 84-97, Jan.-Feb. 2018.

[2]. H. Karkkainen, L. Aarniovuori, M. Niemela and J. Pyrhonen, "Converter-Fed Induction Motor Efficiency: Practical Applicability of IEC Methods," in *IEEE Industrial Electronics Magazine*, vol. 11, no. 2, pp. 45-57, June 2017.

[3]. M. Boesing and R. W. De Doncker, "Exploring a Vibration Synthesis Process for the Acoustic Characterization of Electric Drives," in *IEEE Transactions on Industry Applications*, vol. 48, no. 1, pp. 70-78, Jan.-Feb. 2012.

[4]. L. Aarniovuori, H. Kärkkäinen, A. Anuchin, J. J. Pyrhönen, P. Lindh and W. Cao, "Voltage-Source Converter Energy Efficiency Classification in Accordance With IEC 61800-9-2," in *IEEE Transactions on Industrial Electronics*, vol. 67, no. 10, pp. 8242-8251, Oct. 2020.

[5]. F. C. F. Azevedo and M. N. Uddin, "Recent advances in loss minimization algorithms for IPMSM drives," 2014 IEEE Industry Application Society Annual Meeting, Vancouver, BC, Canada, 2014, pp. 1-9.

[6]. Z. Li, D. O'Donnell, W. Li, P. Song, A. Balamurali and N. C. Kar, "A Comprehensive Review of State-of-the-Art Maximum Torque per Ampere Strategies for Permanent Magnet Synchronous Motors," 2020 10th International Electric Drives Production Conference (EDPC), Ludwigsburg, Germany, 2020, pp. 1-8.

[7]. M. Caruso, A. O. Di Tommaso, F. Genduso and R. Miceli, "Experimental investigation on high efficiency real-time control algorithms for IPMSMs," 2014 International Conference on Renewable Energy Research and Application (ICRERA), Milwaukee, WI, USA, 2014, pp. 974-979.

[8]. A. Bruno, M. Caruso, A. O. Di Tommaso, R. Miceli, C. Nevoloso and F. Viola, "Simple and Flexible Power Loss Minimizer With Low-Cost MCU Implementation for High-Efficiency Three-Phase Induction Motor

Drives," in *IEEE Transactions on Industry Applications*, vol. 57, no. 2, pp. 1472-1481, March-April 2021.

[9]. IEC 61800-9-1. Adjustable speed electrical power drive systems - Part 9-1: Ecodesign for power drive systems, motor starters, power electronics and their driven applications - General requirements for setting energy efficiency standards for power driven equipment using the extended product approach (EPA) and semi analytic model (SAM), 2017.

[10]. IEC 61800-9-2. Adjustable Speed Electrical Power Drive Systems—Part 9-2: Ecodesign for Power Drive Systems, Motor Starters, Power Electronics & Their Driven Applications—Energy Efficiency Indicators for Power Drive Systems and Motor Starters, 2017.

[11]. N. Yogal, C. Lehrmann and M. Henke, "Determination of the Measurement Uncertainty of Direct and Indirect Efficiency Measurement Methods in Permanent Magnet Synchronous Machines," 2018 XIII International Conference on Electrical Machines (ICEM), Alexandroupoli, Greece, 2018, pp. 1149-1156.

[12]. E. B. Agamloh, A. Cavagnino and S. Vaschetto, "Standard Efficiency Determination of Induction Motors With a PWM Inverter Source," in *IEEE Transactions on Industry Applications*, vol. 55, no. 1, pp. 398-406, Jan.-Feb. 2019.

[13]. Caruso, M.; Di Tommaso, A.O.; Lisciandrello, G.; Mastromauro, R.A.; Miceli, R.; Nevoloso, C.; Spataro, C.; Trapanese, M. A General and Accurate Measurement Procedure for the Detection of Power Losses Variations in Permanent Magnet Synchronous Motor Drives. Energies 2020, 13, 5770.

[14]. M. Caruso, A.O. Di Tommaso, R. Miceli, C. Nevoloso, C. Spataro, Uncertainty evaluation in the differential measurements of power losses in a power drive system, Measurement, Volume 183, 2021, 109795, ISSN 0263-2241.

[15]. L. Aarniovuori, H. Kärkkäinen, M. Niemelä and J. Pyrhönen, "PWM-Induced Harmonic Power in 75 kW IM Drive System," 2020 22nd European Conference on Power Electronics and Applications (EPE'20 ECCE Europe), Lyon, France, 2020, pp. P.1-P.9.

[16]. A. Anttila, L. Aarniovuori, M. Niemelä, M. Zaheer, P. Lindh and J. Pyrhönen, "Active Power Analysis of PWM-driven Induction Motor in Frequency Domain," 2021 XVIII International Scientific Technical Conference Alternating Current Electric Drives (ACED), Ekaterinburg, Russia, 2021, pp. 1-6.

[17]. M. Caruso, A.O. Di Tommaso, R. Miceli, C. Nevoloso, C. Spataro, F. Viola, Characterization of the parameters of interior permanent magnet synchronous motors for a loss model algorithm, Measurement, Volume 106, 2017, Pages 196-202, ISSN 0263-2241.

[18]. Busacca, A.; Di Tommaso, A.O.; Miceli, R.; Nevoloso, C.; Schettino, G.; Scaglione, G.; Viola, F.; Colak, I. Switching Frequency Effects on the Efficiency and Harmonic Distortion in a Three-Phase Five-Level CHBMI Prototype with Multicarrier PWM Schemes: Experimental Analysis. Energies 2022, 15, 586.

[19]. https://www.meanwell.com/Upload/PDF/RSP-2400/RSP-2400- SPEC.PDF.

[20]. A. Poorfakhraei, M. Narimani and A. Emadi, "A Review of Modulation and Control Techniques for Multilevel Inverters in Traction Applications," in *IEEE Access*, vol. 9, pp. 24187-24204, 2021.